16

Spatial distribution of eruptive centers about the Idaho National Laboratory

P. H. Wetmore, S. S. Hughes, L. J. Connor, M. L. Caplinger

Regional volcanic hazard investigations require an in-depth understanding of a region's spatial and temporal distribution of volcanic vents and variations in eruption rates. Usually assessments are based solely upon the distribution of vents and eruptive centers exposed at the surface. These assessments commonly assume relatively simple tectono-magmatic settings and evolutions (e.g. Connor *et al.*, 1992; Conway *et al.*, 1998). Hazard studies within tectonically complicated regions, such as the Basin and Range of the western US (e.g. Yucca Mountain, Connor *et al.*, 2000; Valentine and Perry, Chapter 19, this volume), have demonstrated the need for more accurate knowledge of the regional volcanic stratigraphy. In this chapter, we describe an analysis of volcanic hazards that includes this more comprehensive view of volcano stratigraphy. Such detailed investigations, accounting for differential subsidence and the burial of older volcanic features, can vastly improve the accuracy of any volcanic hazard assessment.

The Idaho National Laboratory (INL) comprises several nuclear facilities, including the oldest power reactor in the world (see Chapman *et al.*, Chapter 1, this volume). The INL is located in a region of volcanic hazards stemming from its position on the eastern Snake River Plain (ESRP). The ESRP is one of the most volcanically active regions in North America. Recent volcanism on the plain is characterized by the effusion of very low viscosity lavas. The resulting lava flows are often < 10 m thick, but inundate vast areas, up to 1500 km^2. Volcanism on the ESRP is predominantly monogenetic, meaning that renewed volcanic activity and accompanying lava flows form from new batches of melt and issue from new volcanic vents (see Connor *et al.*, Chapter 3, this volume). Additionally, the ESRP transects but, continues to be structurally affected by, the northern Basin and Range Province. Thus, volcanic hazard assessments must consider, not only the temporal rates of volcanic activity, the potential magnitudes of eruptions, and the potential distribution of future volcanic vents from which lavas effuse, but also the poten-

tial complications associated with active normal faulting (e.g. differential vertical motions).

An accurate understanding of the spatial variability in recurrence and accumulation rate of volcanism in the central ESRP at and near the INL is important due to the presence of nuclear reactors and other highly sensitive facilities located within this US Department of Energy site. Most hazard assessments for the region have worked under the assumption that volcanism is focused into NW-trending volcanic rift zones (VRZs; Hackett and Smith, 1994). However, a two decade long extensive study of the stratigraphy at depth beneath the INL (Anderson *et al.*, 1996, 1997; Hughes *et al.*, 2002a; Champion *et al.*, 2002) provides a unique opportunity to assess the spatial and temporal evolution of magmatism within one of the most productive basaltic volcanic fields in North America. These investigations reveal the locations of ≈ 50 buried eruptive centers/vents, and led to identification of differential subsidence of various parts of the plain. In this chapter we employ the results of these studies to illustrate how the distribution of exposed vents in the central portion of the ESRP results from the complex interplay between spatial variability in the recurrence of volcanic events, accumulation of lava flows, and differential subsidence and sedimentation.

In the following sections we describe the distribution of exposed and buried vents at and near the INL, the spatial variability of vent density and basalt accumulation, and the role and various scales of subsidence of the ESRP with potential connections to faulting in the adjacent Basin and Range Province. We then relate the distribution of volcanic vents and their preservation at the surface to the competing effects of spatial variations in magma productivity and subsidence. Finally, we demonstrate how including these vents, now buried in the subsurface, changes models of spatial density of vent distribution, and hence the volcanic hazard assessment for the INL.

16.1 Geology of the ESRP and the INL region

The ESRP of southeastern Idaho is a major tectonic depression, under-filled with late Cenozoic volcanic and sedimentary strata (Figure 16.1). The Plain formed in the wake of the Yellowstone hot spot (Pierce and Morgan, 1992) as rhyolitic volcanism ceased and basaltic volcanism flared-up. Basaltic volcanism of the Plain is dominated by low-volume ($< 6\,\mathrm{km}^3$) monogenetic eruptions (Kuntz *et al.*, 1986, 1992) with some evidence for isolated larger volume ($8-20\,\mathrm{km}^3$) flows during the late Pleistocene (Wetmore *et al.*, 1997; Wetmore, 1998; Scarberry, 2003).

Basaltic volcanism of the ESRP is traditionally inferred to be asymmetrically distributed into a series of narrow, curvilinear and NW-trending volcanic rift zones (VRZs), based on the distribution of exposed eruptive centers (Kuntz, 1977a, 1977b;

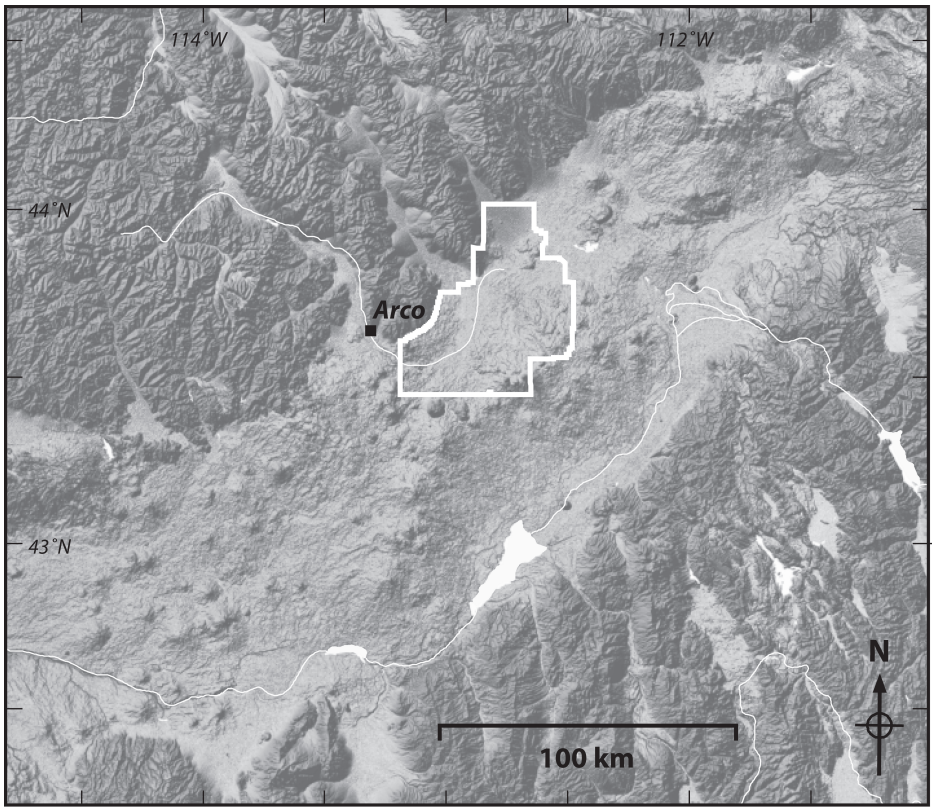

Fig. 16.1. This digital elevation model (DEM) of the ESRP shows its unique geology, with subdued topography compared with the surrounding fault-block mountain ranges. The ESRP itself is armored by low viscosity lava flows that produce an overall smooth surface. The Idaho National Laboratory (INL) is centrally located and outlined in white. The Axial Volcanic Zone is a curvilinear string of large volcanoes that form a low ridge, trending NE along the SE border of the INL. The town of Arco is indicated for reference.

Kuntz *et al.*, 1992). Boundaries of these VRZs are outlined in Figure 16.2. Many of these VRZs appear to be continuations of range-front faults of the Basin and Range Province to the north of the plain (e.g. Arco–Big Southern Butte VRZ and the Big Lost River fault zone). Similar to many other such basaltic volcanic fields of the Basin and Range Province, the VRZs of the ESRP are characterized by aligned vents, non-eruptive fissures, and small offset normal faults that are approximately parallel to the margins of the rift zones and the traces of the range-front faults in the adjacent Basin and Range (Kuntz *et al.*, 1992, 1994, 2002). Throughout the remainder of this chapter the VRZs will be utilized as geographic reference points. We will return to the issue of their viability as zones of focused magmatism in the discussion section.

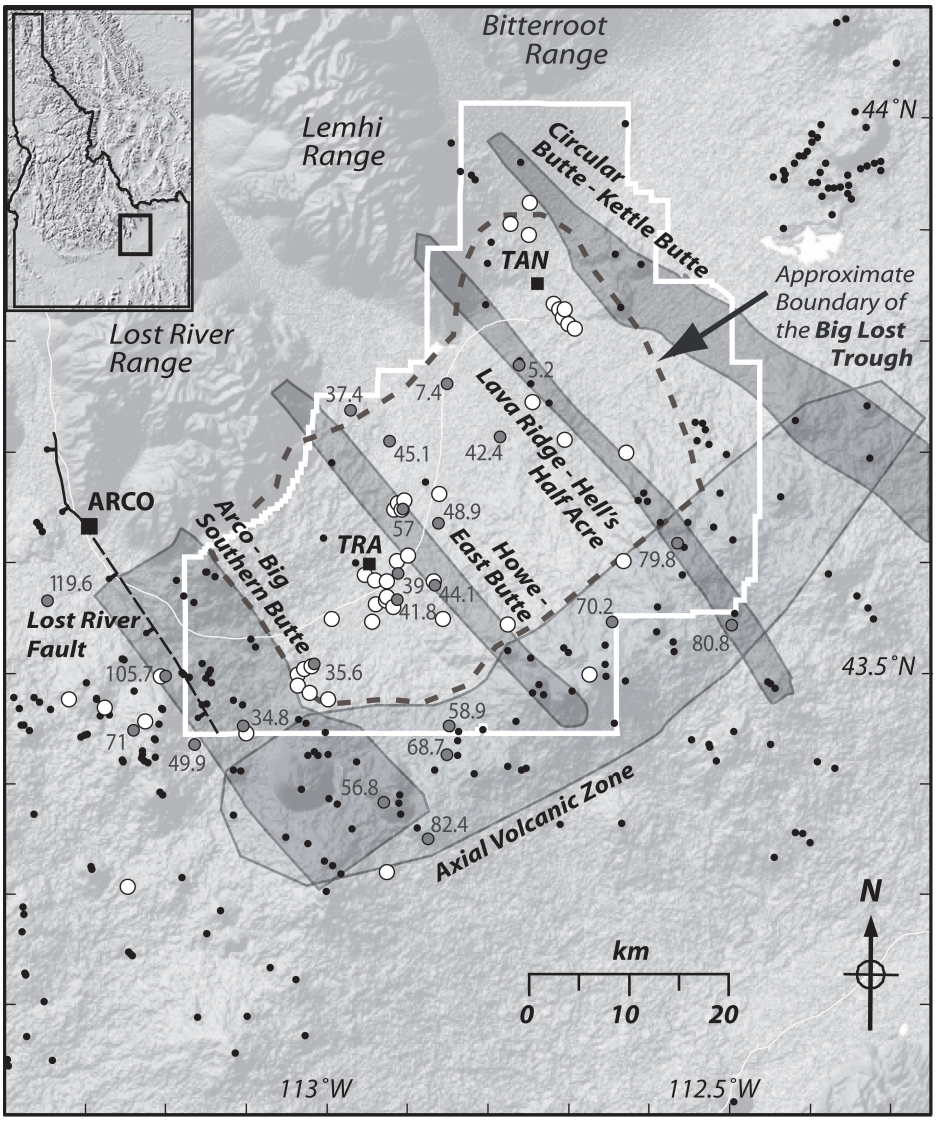

Fig. 16.2. This map of the central ESRP shows the INL border outlined in white, labeled boundaries of the VRZs and the Axial Volcanic Zone, exposed vents as black dots, inferred vents in the subsurface as white circles, and the Big Lost Trough enclosed by a circular dashed line within the INL border. The distribution of exposed and inferred vents from Anderson and Liszewski (1997) shows that while many exposed vents lie within the VRZs described by Kuntz *et al.* (2002), many inferred vents lie between these zones. Gray circles are labeled with accumulation rates of basalt (mm a^{-1}) averaged over the last 600 ka that demonstrate some spatial variability in the accumulation of basalt, especially between the Axial Volcanic Zone and the Big Lost Trough. The black line tracing the Lost River Fault has barbs on the hanging wall. The dashed portion is the inferred position within the ESRP based on the location of small offset fault scarps in the Arco–Big Southern Butte VRZ (Kuntz *et al.*, 1994).

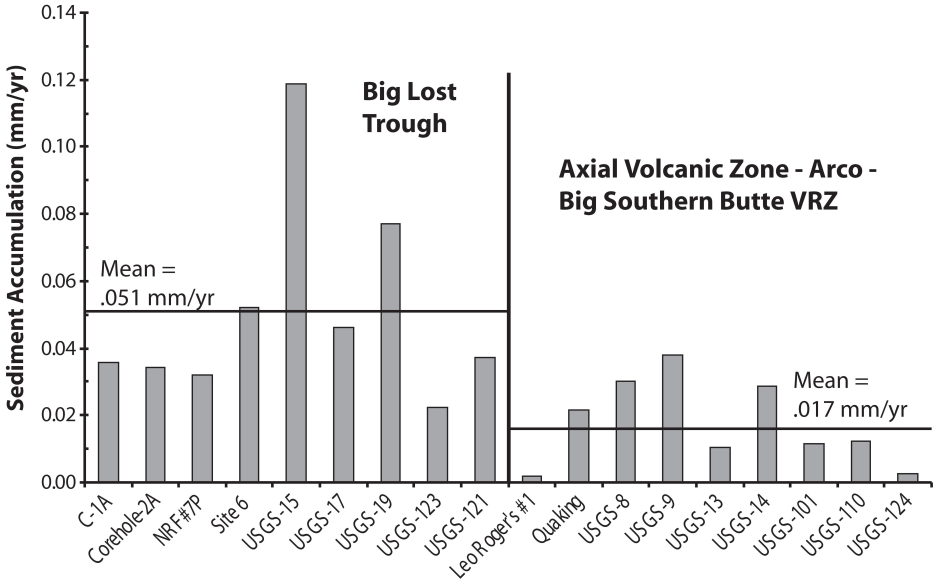

Fig. 16.3. Bars show sediment accumulation rates for selected wells within the Big Lost Trough and the Arco–Big Southern Butte VRZ and the Axial Volcanic Zone. Rates are calculated using stratigraphic distribution, thickness and age data from Anderson *et al.* (1996, 1997). Vertical bar separates wells from the two subprovinces.

The INL is located within the central portion of the ESRP (as shown in Figures 16.1 and 16.2), and is transected, from SW to NE, by four inferred VRZs, Arco–Big Southern Butte, Howe–East Butte, Lava Ridge–Hell's Half Acre, and Circular Butte–Kettle Butte. Three of these VRZs, Arco–Big Southern Butte, Lava Ridge–Hell's Half Acre and Circular Butte–Kettle Butte, appear to be continuations of range front faults. Additionally, the Axial Volcanic Zone approximately parallels and overlaps the southern and SE boundary of the site.

Most of the INL occupies a low-relief Pleistocene–Holocene depositional basin known as the Big Lost Trough (Gianniny *et al.*, 1997, 2002). This basin (outlined in Figure 16.2) is bounded by the relatively high topography of the Arco–Big Southern Butte VRZ on the southwest, the Axial Volcanic Zone on the southeast, the Circular Butte–Kettle Butte VRZs to the NE, and the Basin and Range Province to the NW. It is transected by both the Howe–East Butte and Lava Ridge–Hell's Half Acre VRZs in its central and NE portions, respectively. Relative to the bounding volcanic zones, sedimentation rates are as much as two to three times higher in the Big Lost Trough, as shown in Figure 16.3.

The Axial Volcanic Zone (Figure,16.2) is another region of the ESRP where volcanism is believed to be focused (Hackett and Smith, 1994). This feature parallels

the axis of the ESRP and is most prominent near the central portion of the Plain along the southeastern boundary of the INL. Eruptions of the Axial Volcanic Zone lavas have erected a low but massive topographic high, which is clearly visible on the DEM (Figure 16.1). Here the Axial Volcanic Zone serves as a drainage divide preventing rivers flowing south out of the Basin and Range to the north from crossing the plain. Rather, these rivers are diverted into large ephemeral lakes (e.g. Lost River Sinks) whose waters seep into the Snake River Plain Aquifer (Bartholomay *et al.*, 2002). The Axial Volcanic Zone is also a region of the plain where highly differentiated magmas are extruded, such as those representing the high silica rhyolite domes and intermediate composition Cedar Butte (Hayden, 1992; McCurry *et al.*, 1999, 2008).

As a result of the need to remediate contamination of the Snake River Plain Aquifer, geophysical, geochronological, and geochemical/petrological data collected from several hundred wells and a few dozen coreholes help to define the subsurface distribution and stratigraphy of lava flows in the vadose zone and uppermost part of the Snake River Plain Aquifer at and near the INL (Anderson, 1991; Anderson and Bartholomay, 1995; Anderson and Bowers, 1995; Anderson and Lewis, 1989; Anderson and Liszewski, 1997; Anderson *et al.*, 1996, 1997). The correlations of subsurface lava flows made by Anderson and co-workers were employed by Anderson and Liszewski (1997) and Wetmore (1998) to establish the locations of buried eruptive centers in the central portion of the ESRP. In general, this was accomplished through the construction of isopach and structural contour maps of upper and lower flow surfaces for each identified and regionally correlated flow package observed in the coreholes and wells. A full description of their methods for identifying the positions of buried eruptive centers can be found in those references. In addition to locating eruptive centers, the stratigraphic data of Anderson *et al.* (1996) were also used by Wetmore (1998) and Champion *et al.* (2002) to define regions of differential subsidence and uplift in the area of the INL. Similarly, Blair (2002) cited variation of the elevations of correlative sedimentary units between cores from the southern portion of the INL as evidence of post-depositional differential subsidence of the Big Lost Trough.

16.2 Spatial variation in basaltic magmatism

Within the central portion of the ESRP, 232 exposed eruptive centers have been located near the INL (Kuntz *et al.*, 1994). These are primarily confined to the Arco–Big Southern Butte VRZ, the Axial Volcanic Zone, and clusters of centers around the Test Area North (TAN) facility (locations are plotted in Figure 16.2). Within the central portion of the INL, eruptive centers and their encompassing shields are limited in number and prominence as they tend to be partially buried by

younger flows and sediments. In the east-central and northern portions of the INL, a NW-trending alignment of vents, west and southwest of the TAN facility, defines the Lava Ridge–Hell's Half Acre VRZ. East and southeast of the TAN facility are three vents (Antelope Butte, Circular Butte, and an unnamed butte) that form the northern end of the Circular Butte–Kettle Butte VRZ.

Ages of these exposed eruptive centers reveal a pattern of younger (i.e. those less than ~ 200 ka) eruptive centers restricted to the Axial Volcanic zone (Kuntz *et al.*, 1994). The oldest eruptive centers within the four VRZs are concentrated in the NW portions of the zones (> 500 ka for the Arco–Big Southern Butte and > 730 ka for the other three VRZs). The youngest centers are present to the southeast where the VRZs intersect the Axial Volcanic Zone. The isolated and partially buried centers in the central part of the INL, especially those near INTEC, a facility in the middle of the site, are relatively old at ~ 650 ka (Anderson and Liszewski, 1997).

16.2.1 Inferred eruptive centers

Two recent studies of the basaltic flow field architecture in the subsurface of the central ESRP at and near the INL (Anderson and Liszewski, 1997; Wetmore, 1998) identify ≈ 47 additional eruptive centers concealed by younger lava flows and sediment (locations in Figure 16.2). While the methods for identifying the locations of vents concealed in the subsurface are not explicitly described by Anderson and Liszewski (1997), it is clear, based on comparison with well and corehole data from Anderson *et al.* (1996), that the vent location for any particular unit closely coincides with the region of thickest basalt accumulation where that unit is correlated in wells or coreholes. Wetmore (1998), using the Anderson *et al.* (1996) data, generated isopach and structural contour maps of the upper and lower surfaces of the flow units, to identify areas of greatest flow field thickness. These areas are coincident with the higher elevation of the upper surface to locate concealed eruptive centers.

The majority of the 47 vents identified by Anderson and Liszewski (1997) are located near facilities in the southwestern portion of the INL and south of the TAN facility (Figure 16.2). Wetmore (1998) identified 32 vents within the southern INL area. In general, between the two studies, the differences in the locations of vents from the same basalt flow group are small (< 2 km). Therefore, those inferred by Anderson and Liszewski (1997) will be used in the analyses of vent distribution in the following sections, due to the broader area investigated in their study.

Throughout the central portion of the INL nearly all vents ranging in age from ~ 650 – 247 ka are concealed in the subsurface. Only vents from the largest flow field (i.e. the *I* flow, 626 + 67 ka; Anderson *et al.*, 1997) and the youngest extrusions

(i.e. the *B* flow, 221 + 2 ka; Anderson *et al.*, 1997) are exposed at the surface within the southern portion of the INL.

One way to visualize the distribution of vents near the INL is to generate a histogram plot relating the number of vents to distance across or along the ESRP (Figure 16.4). We overlaid a grid onto the distribution map shown in Figure 16.2 and tabulated the number of vents in each box as a function of distance from the margin of the Plain (Figure 16.4a) and as a function of distance from the southwestern edge of the map (Figure 16.4b–c). Vents were counted in bins that were 5 km on a side. The vents shown in these plots lie between the NW margin of the ESRP and ≈ 25 km SE of the axis of the plain, and from ≈ 20 km SW of the Lost River Fault/Arco–Big Southern Butte VRZ and ≈ 5 km NE of the Beaverhead fault. The overlain grid is oriented with one axis approximately parallel to the axis of the ESRP, while the other axis is approximately parallel with the trends of the VRZs and the range-bounding faults of the Basin and Range Province to the north.

Figure 16.4a plots number of vents with distance from the NW margin of the ESRP, including the vents inferred to exist in the subsurface. In this plot there are relatively few vents in the NW part of the ESRP as the grid extends ≈ 15 km beyond the actual margin in the SW portion of the map area (Figure 16.2), so the plot also includes those vents near Arco and the TAN facility. Throughout the middle portion of the transect (i.e. 20–70 km) the average number of vents per bin is ≈ 20. Relatively few vents occur SE of the Axial Volcanic Zone, which Kuntz (1992) attributes to a low-density barrier formed by the Taber caldera, a buried rhyolitic eruptive center associated with the passage of the Yellowstone hot spot (Pierce and Morgan, 1992).

Figure 16.4b–c plot number of vents with distance from a SW to NE transect that crosses three faults and four VRZs. Figure 16.4b uses all vents, including those from the Axial Volcanic Zone, while Figure 16.4c excludes vents from the latter volcanic zone to emphasize the variability within and between VRZs and as a function of distance from faults. Figure 16.4c does not seem to support the inference that VRZs represent zones of focused volcanism since they are, in all cases, not coincident with the most prominent vent clusterings or surrounded by regions of reduced vent clustering. Similarly, the distribution of volcanoes relative to the location of faults is inconsistent. For example, the Lost River fault bisects a region with an average of 11.5 exposed vents per 5 km, while there are no exposed vents within 5 km SW or NE of the Lemhi fault. Between the two faults, however, is a region with relatively few exposed vents but an average of ≈ 5 vents per 5 km inferred to be present in the subsurface of the ESRP.

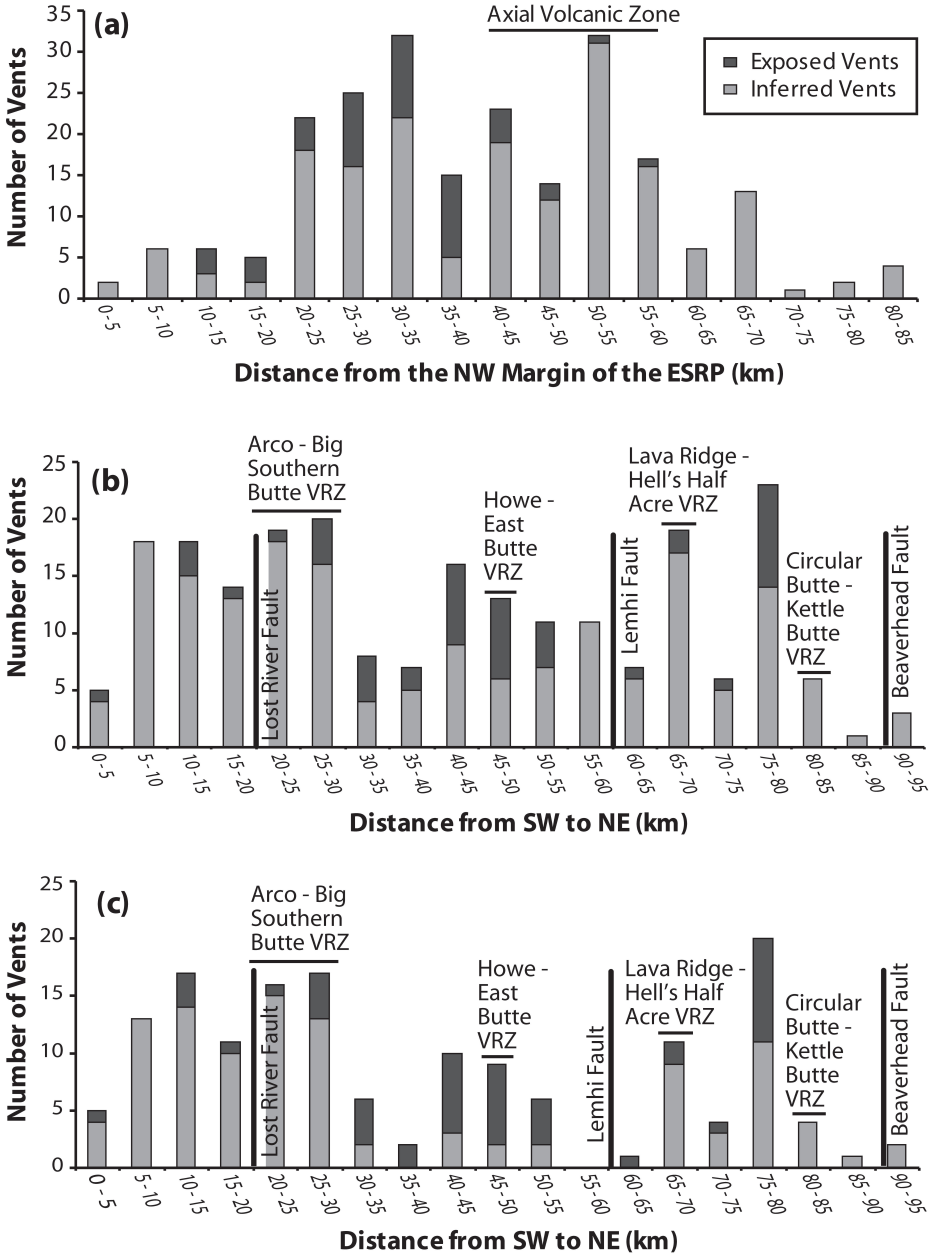

Fig. 16.4. The histograms show the distributions of exposed and inferred vents at and near the INL, inferred locations from Anderson and Liszewski (1997). Plot (a) shows the distribution of vents from the NW margin of the Plain to the Axis and beyond. Plot (b) shows vent distributions from SW of the Arco–Big Southern Butte VRZ to NE of the Circular Butte–Kettle Butte VRZ. Plot (c) is identical to plot (b) but excludes vents within the Axial Volcanic Zone.

16.2.2 Regional density estimation using Gaussian smoothing

An alternative way to view the clustering and regional spatial distribution of volcanic vents located within the ESRP is by kernel density estimation based on vent locations. A robust and unbiased approach uses a Gaussian kernel function and an optimized bandwidth selector algorithm to calculate the spatial density across an area. Since spatial density is highly sensitive to the smoothing bandwidth used in the calculation, an optimal bandwidth is chosen by an unbiased algorithm that is based solely on the vent locations, in other words bandwidth selection is data-driven. This method is discussed in detail by Connor and Connor (Chapter 14, this volume).

For the exposed vents within the ESRP, the derived optimal bandwidth, **H**, is a 2×2 matrix of values given by:

$$\mathbf{H} = \begin{bmatrix} 122 & 79 \\ 79 & 87 \end{bmatrix}$$

which specifies the amount of spatial variation in the E−W and N−S directions and the overall trending direction of the data. The square root of the bandwidth matrix gives the following matrix:

$$\sqrt{\mathbf{H}} = \begin{bmatrix} 10.2 & 4.3 \\ 4.3 & 8.3 \end{bmatrix}$$

which corresponds to the amount of smoothing in km. Specifically, for exposed vents in the ESRP, the optimal smoothing distance is ≈ 10.2 km in an E−W direction, ≈ 8.3 km in a N−S direction, with a positive overall clustering trend from the SW towards the NE at $\approx 45°$ from north.

Similarly, the optimized bandwidth matrix, **H**, for calculating the spatial density of vents based on exposed and subsurface vents is given by:

$$\mathbf{H} = \begin{bmatrix} 130 & 82 \\ 82 & 88 \end{bmatrix}$$

and the square root of this matrix is given by:

$$\sqrt{\mathbf{H}} = \begin{bmatrix} 10.5 & 4.4 \\ 4.4 & 8.1 \end{bmatrix}$$

which corresponds to an optimal smoothing distance of $\approx$10.5 km in the E−W direction, ≈ 8.1 km in the N−S direction, with the overall clustering exhibiting the same SW to NE trend. Overall, the addition of subsurface vents to the exposed vent population does not significantly change the dimensions of the optimal smoothing bandwidth for this enlarged population. To see the unique smoothing effect of this

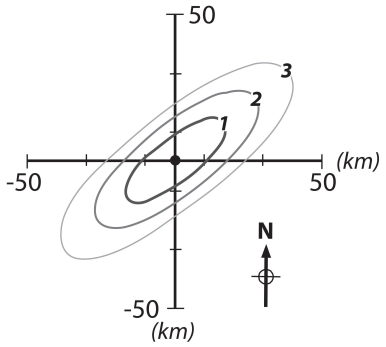

Fig. 16.5. This plot illustrates the unique Gaussian smoothing effect of the optimal bandwidth matrix centered around one vent. The area within the contours (from inside to outside) represent 68%, 95%, and 99.7% of the total spatial density, that is 1, 2, and 3 standard deviations from the mean spatial density. A map is generated by summing this smoothing effect for each vent and then normalizing the grid to create a probability density surface (i.e. the surface integrates to one) which is then contoured as in Figures 16.5 and 16.6.

bandwidth matrix, a spatial density map was calculated based on a single vent centrally located within the ESRP region. The results are shown as an x−y plot in Figure 16.5.

A spatial density estimation across the entire ESRP region, an approximate 325 km by 280 km area (which includes the INL), is calculated by summing the smoothing effect of the bandwidth around each event in the dataset and then normalizing the entire grid so that the vent density integrates to 1. Figure 16.6 shows the density grid calculated for exposed vents within the ESRP contoured at quartile intervals (i.e. 25%, 50%, 75%) and intervals representing 95% and 99% of the entire spatial density (i.e. includes approximately two and three standard deviations from the mean spatial density). Notice the area of low density within the central region of the INL in Figure 16.6.

Figure 16.7 shows the spatial density variation across the region based on exposed and subsurface vents. The obvious difference between the two spatial density maps (Figures 16.6 and 16.7) is the disappearance of the low density area that was centrally located within the INL boundary, obviously due to the inclusion of the subsurface vents in the analysis. This difference can be quantified by differencing the two spatial density grids, thereby creating a third grid which illustrates the relative differences in density (Figure 16.8). An interesting question is, does the spatial density map represent an accurate estimation of the probability of volcanic hazard to the INL facility and does the inclusion of subsurface (inferred) vents increase that hazard?

Based on these regional spatial density maps, contours of equal density are

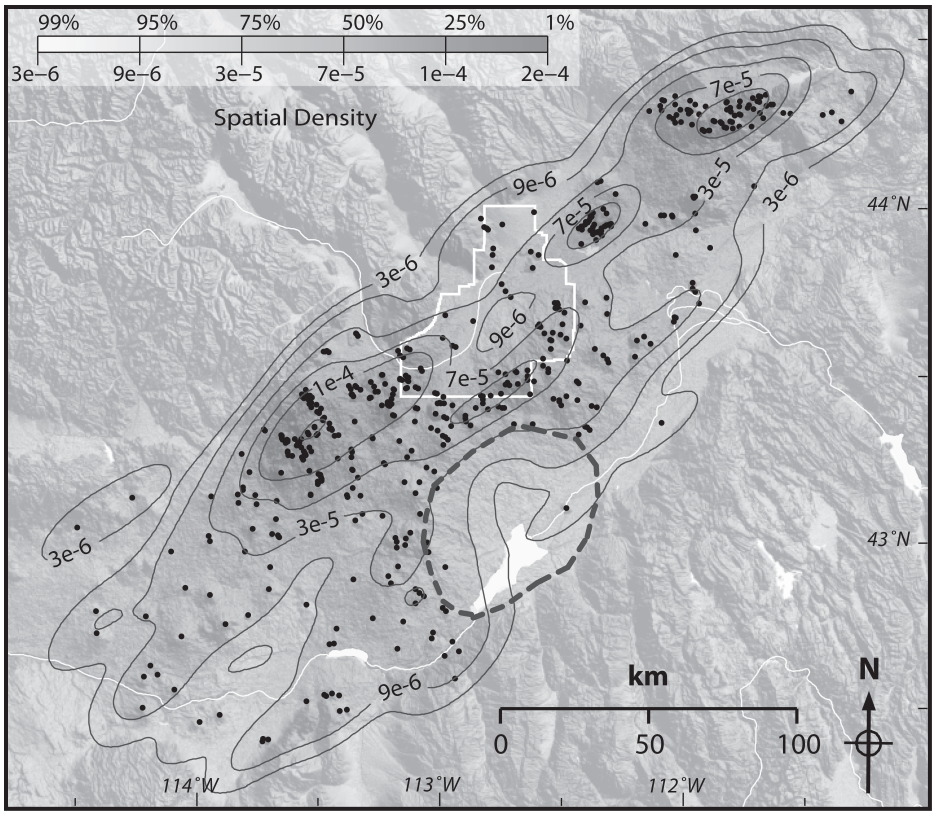

Fig. 16.6. This contour plot of the spatial density estimation of exposed vent locations within the ESRP is based on a grid that was calculated using a Gaussian kernel function and an optimal $2\,x\,2$ smoothing bandwidth matrix. The contours indicate 25%, 50%, 75%, 95% and 99% of the total spatial density (e.g. 50% of the total spatial density falls within the $7x10^{-5}$ contour). Black dots represent the locations of exposed vents. The INL boundary is outlined in white. Notice the centrally located hole of lower spatial density within the center of the INL due to the absence of exposed vents. The dark gray (dashed) circle represents the approximate location of Taber caldera (Pierce and Morgan, 1992).

mostly elongate in a NE direction, approximately parallel to the axis of the ESRP. Most prominent are three high intensity zones located adjacent to the NW margin of the ESRP. The Axial Volcanic Zone makes a fourth, less intense zone, off of the main trend. These regional spatial density maps do not appear to capture the pattern of discrete NW trending zones of volcanism, perpendicular to the ESRP, as shown by the locations of the VRZs in Figure 16.2.

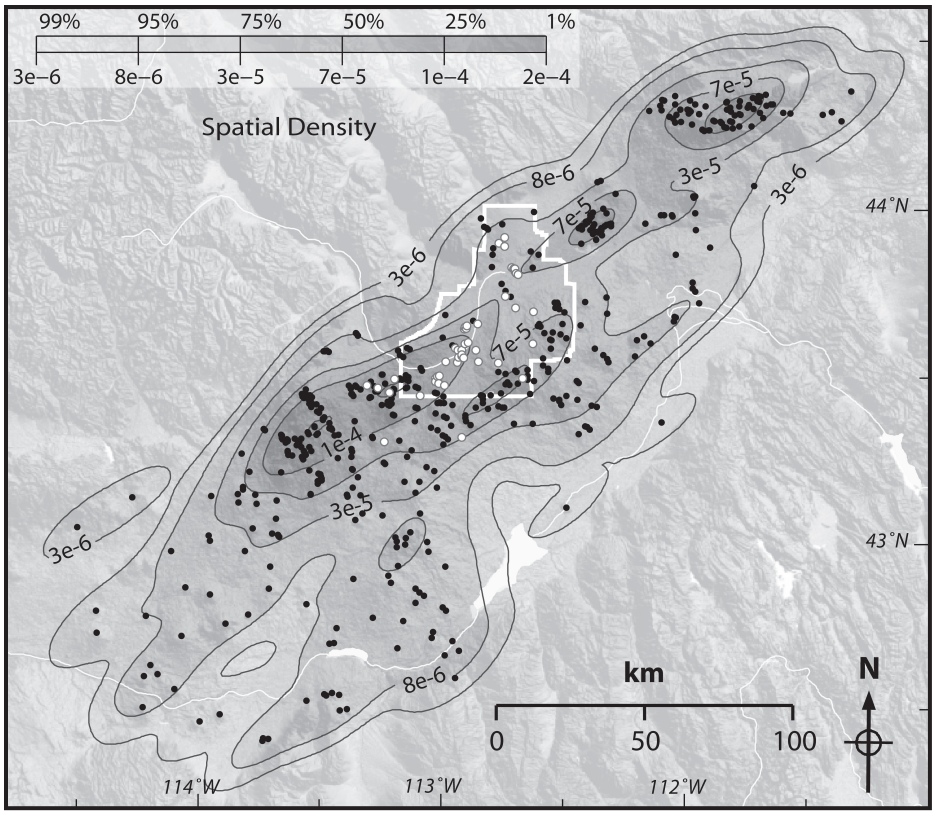

Fig. 16.7. This contour plot of spatial density was based the population of exposed (black dots) and subsurface (inferred) vent locations (white circles) within the ESRP. This map was calculated and contoured as described in Figure 16.5. Notice the change in contours within the center of the INL (white lined boundary). The hole of lower spatial density, apparent in Figure 16.5, is no longer evident due to the inclusion of subsurface (inferred) vent locations in the spatial density calculation.

16.2.3 Spatial variations in the rate of basalt accumulation

Since ~ 650 ka the overall average accumulation rate of basalt at and near the INL has been ~ 58 km^3 100 ka^{-1} in volume and ~ 49 m 100 ka^{-1} in thickness (Wetmore *et al.*, 1997; Wetmore, 1998). However, the accumulation rate is highly variable throughout the INL as illustrated by the paleomagnetic interpretations of Champion *et al.* (2002). Within the boundaries of the INL, they observe dramatic gradients in the rate of basalt accumulation from corehole to corehole (e.g. a change of 47 m 100 ka^{-1} over 13 km near the Test Reactors Area (TRA)). Perhaps most significant is their observation that accumulation rates increase toward the axis of the ESRP (i.e. with proximity to the Axial Volcanic Zone) while the recurrence interval between eruptive events decreases.

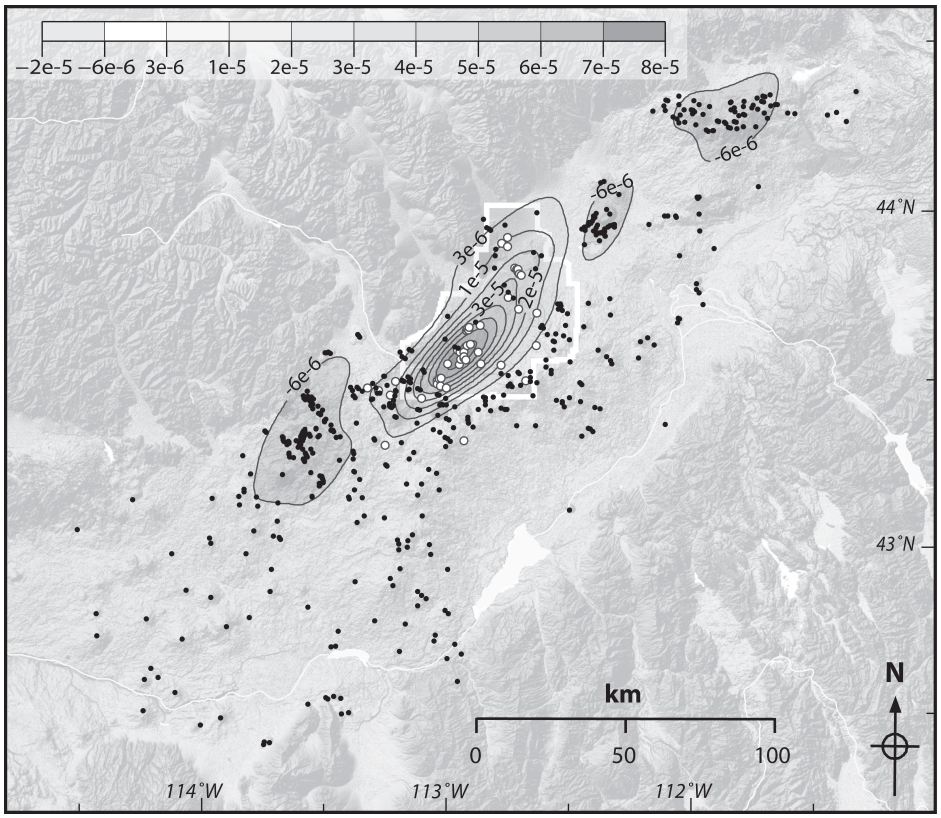

Fig. 16.8. This map shows the difference between the spatial density map in Figure 16.5 and the spatial density map in Figure 16.6. The difference is contoured at a 1×10^{-5} km^2 interval. The centrally located positive anomaly is caused by an increase in spatial density due to the inclusion of subsurface vents . The smaller negative anomalies to either side of the "high" are a relative effect due to the centrally located positive anomaly.

Figure 16.2 shows locations and rates of basalt accumulation (in mm a^{-1}) from select wells and coreholes about the INL. Spatial variability in the accumulation of basalt reveals an overall pattern that is generally consistent with that described by Champion *et al.* (2002). Specifically, an increase in the rate occurs toward the southeast, i.e. toward the Axial Volcanic zone; however, a general increase is evident toward the Arco−Big Southern Butte VRZ, with the highest rates observed southwest of the zone. Accumulation rates from wells within the Big Lost Trough are, on average, half as large as those from the two bounding volcanic zones (Figure 16.9).

It should be noted, however, that a substantial hiatus in volcanism occurred during the late Quaternary throughout much of the area shown in Figure 16.2, and certainly where the wells were drilled from which accumulation data were derived.

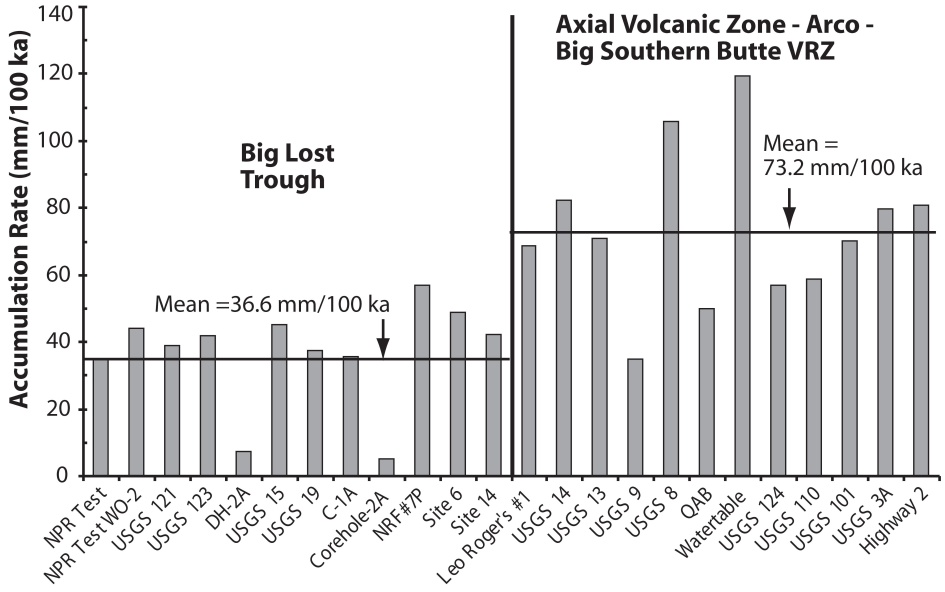

Fig. 16.9. This plot compares accumulation rates of basalt measured from select wells and core holes located within two regions near the INL, the Big Lost Trough and the Arco−Big Southern Butte VRZ and Axial Volcanic Zone. Rates are calculated using data from Anderson *et al.* (1996, 1997).

Within much of the southern Big Lost Trough, for example, no eruption has occurred for at least the last ~ 218 000 a. Most of the Arco−Big Southern Butte VRZ and the northern Big Lost Trough experienced a much longer hiatus, ranging from 300 ka to almost 500 ka (Kuntz *et al.*, 1994; Anderson *et al.*, 1997). Younger flows cover some portions of the Axial Volcanic Zone, but none are younger than ~ 95 ka in any of the wells (Anderson *et al.*, 1996, 1997).

16.3 Subsidence and the Big Lost Trough

Several lines of evidence demonstrate that the ESRP has and probably still is, subsiding relative to the adjacent Basin and Range Province. Additionally, a second order subsidence is also observed locally within the Plain. Whereas the former subsidence is likely related to large-scale flexure due to the passage of the region over the Yellowstone Hot Spot and the consequential formation of a mafic mid-crustal sill, the latter appears to be the consequence of Basin and Range faulting continuing into the ESRP.

16.3.1 Subsidence relative to the surrounding Basin and Range

One of the most striking aspects of the ESRP is that it is a relatively low-standing region transecting the relatively high-standing northern Basin and Range Province. Rivers flow toward the Plain from both the NW and SE sides, and the ridge lines of most ranges appear to rotate into the ESRP along its margins. McQuarrie and Rodgers (1998), studying the rotation of Mesozoic fold hinges from sub-horizontal orientations into steep SE plunges along the NW margin of the Plain, demonstrated as much as 8.5 km of subsidence of the ESRP relative to the adjacent Basin and Range Province. The amount of subsidence adjacent to the INL ranges from 4.5−8.5 km.

McQuarrie and Rodgers (1998) argue that the subsidence is related to flexure caused by a mid-crustal load, namely, a mafic sill or sill complex, between 17−25 km thick, that formed during the passage of the hotspot under this region of the ESRP. While most of the subsidence is inferred to have occurred prior to ~ 6.6 Ma, even before much of the rhyolitic volcanism in the area of the INL, the Plain has subsided an additional 1.5 km since that time.

16.3.2 Local subsidence and basin formation

On a finer scale the ESRP is a mosaic of small basins and subtle topographic ridges (e.g. the Axial Volcanic Zone and Arco−Big Southern Butte VRZ as illustrated by the DEM in Figure 16.1). Wetmore (1998) first suggested that one of these small basins (the Big Lost Trough) formed as a result of differential subsidence based on observations of the subsurface basalt stratigraphy at and near the INL. Wetmore noted that some of the distal portions of lava flows observed in wells and cores within the Arco−Big Southern Butte VRZ were at elevations 120−200 m higher than those of their vent areas located to the east in the Big Lost Trough and the northern portion of the Axial Volcanic Zone. In contrast, there is no evidence for differential vertical movements between the Big Lost Trough and the Axial Volcanic zone. Blair (2002) also noted that the elevations of lake beds in coreholes from the INL exhibits between 120−220 m of elevation change, an observation that, Blair argues, requires post-depositional differential subsidence.

Wetmore (1998) suggested several possible causes for the observed subsidence of the Big Lost Trough relative to the Arco−Big Southern Butte VRZ, including the extension of faulting from the Basin and Range onto the ESRP and movement on ring faults associated with the calderas of the Heise volcanic field (a precursor to the Yellowstone caldera). Wetmore *et al.* (1999) and Blair (2002) both argued, however, that slip on the southern continuation of the Big Lost River fault onto the Plain best explains the observed subsidence. Furthermore, Kuntz *et al.* (2002) recently suggested that a series of small off-set faults (5−10 m) in the Arco−Big

Southern Butte VRZ, which have been described as dike-induced features (e.g. Hackett and Smith, 1992), are most likely the on-plain expression of the Big Lost River fault.

16.4 Discussion

The spatial analysis of exposed and the inferred subsurface vents presented here indicate that, although NW-trending vent alignments are apparent in some regions (Kuntz *et al.*, 1992; Hughes *et al.*, 2002a, 2002b) the concept of volcanic rift zones is a questionable characterization of ESRP magmatism. Rather, the data support an interpretation that magmatism is focused into NE-trending elongate zones that approximately parallel the axis of the Plain and are located adjacent to the NW margin. Furthermore, the preservation of the vents at the surface is not solely related to spatial variations in the focus of volcanism (i.e. the volcanic rift zone concept), but rather is a function of the interplay between the spatial variability of volcanism, differential subsidence and burial by sediments and subsequent volcanic rocks. In this section we will use the descriptions of the vent distributions, regional densities, accumulation rates, and differential subsidence to address two fundamental questions. How do the spatial variations in vent distributions, accumulation rates, and subsidence result in the distribution of exposed vents seen at the surface today in the southern INL? What is driving the spatial variability in these aspects of central ESRP tectono-magmatism?

16.4.1 Spatially variable volcanism and differential subsidence

In the southern portion of the INL topography and the distribution of exposed vents clearly define the Arco–Big Southern Butte VRZ, Axial Volcanic Zone, and the Big Lost Trough (Figure 16.1). However, the assumption that vent distribution relates solely to the spatial distribution of volcanism between these three parts of the Plain is unsupported by the preceding analysis. For example, when buried vents from the southern Big Lost Trough are taken into account the density of vents in that area is approximately as high as that to the west and south (Figure 16.7). The density of vents in the southern INL, in fact, does not exhibit significant gradients between these three regions of the ESRP.

The accumulation rates of basalt in the area of the southern INL do vary between the regions, but do not faithfully define their boundaries. Medium rates within the Big Lost Trough ($\sim 35\,\mathrm{m}\,100\,\mathrm{ka}^{-1}$) are also observed in wells in the eastern portion of the Arco–Big Southern Butte VRZ (Figure 16.2), but are much less compared to those west of the rift zone and within the Axial Volcanic Zone ($\sim 60 - > 100\,\mathrm{m}\,100\,\mathrm{ka}^{-1}$).

In general, the descriptions of the subsidence characterizing the southern INL combined with the spatial variations in the distributions of vents and accumulation rates explains the ultimate distribution of exposed vents. Specifically, the subsidence of the Big Lost Trough has resulted in the burial of nearly all vents, although no major change in the vent distribution or rate of basalt accumulation between the Arco–Big Southern Butte VRZ and the Big Lost Trough can be documented. By contrast, vents within the volcanic rift zone have been uplifted and preserved without being buried by subsequent lavas or sediment. This is also supported by the observation that the oldest basaltic rocks at the tops of most wells and coreholes in the Big Lost Trough are ~ 200 ka younger than those at the surface in the Arco–Big Southern Butte VRZ (Kuntz *et al.*, 1994; Anderson and Liszewski, 1997). The lack of any significant topographic change between the Arco–Big Southern Butte VRZ and the Axial Volcanic Zone (elevations range between 1600–1650 m, also see Figure 16.1), although the latter too has subsided relative to the former, is explained by the fact that topography is maintained by accumulation rates that are twice as much as off-axis rates. This, too, is supported by the observation that many parts of the Axial Volcanic Zone are covered by flows much younger than the youngest flows in the Big Lost Trough (~ 221 ka; Anderson and Liszewski, 1997) and Arco–Big Southern Butte VRZ (Kuntz *et al.*, 1994).

West of the Arco–Big Southern Butte VRZ, well correlations reveal the highest accumulation rates, but this area is topographically equivalent to that of the rift zone and the Axial Volcanic Zone (~ 1600 m). This may be explained if the area west of the rift zone and east of Craters of the Moon lava field (Figure 16.2) experienced subsidence associated with slip on the continuation of the Lost River fault onto the ESRP, similar to the explanation for subsidence in the Big Lost Trough (Wetmore *et al.*, 1999; Blair, 2002). In this case, however, the subsided block is located on the hanging wall of the Lost River fault, and basalt accumulation was high enough to keep up with subsidence. The location of the trace of the Lost River fault likely coincides with the zone of small offset fault scarps (2–10 m) within the Arco–Big Southern Butte VRZ (Figure 16.2; Kuntz *et al.*, 1994, 2002). Elevated rates of basalt accumulation in this part of the ESRP derive from the combination of proximity to the northern Great Rift VRZ (i.e. Craters of the Moon) as well as the possibility that this region was subsiding, forming a relatively low area adjacent to an area of high lava output.

16.4.2 Underlying cause(s) of spatially variable volcanism

There are a few specific conclusions that can be made concerning the underlying causes of the spatial variability in ESRP volcanism based on data presented herein. The most significant conclusion is that upper crustal structures (e.g. range-

bounding faults of the Basin and Range Province) do not appear to play a fundamental role in the distribution of basaltic volcanism.

The spatial intensity of basaltic volcanism on the ESRP reaches a maximum in three NE trending elongate zones adjacent to the NW margin of the Plain, as well as the Axial Volcanic Zone (Figure 16.7). Not only are the orientations of these high intensity magmatism zones normal to the trends of the range-bounding faults, they appear to transect the extrapolations of those structures onto the Plain without being affected. For example, the high-intensity zone extending NE from Craters of the Moon to the southern INL crosses the Lost River fault and continues well into the southern Big Lost Trough. While the distribution of basaltic volcanism does not seem to be significantly affected by upper crustal structures, it is affected by the ambient regional stress field, as noted by the orientation/alignment of multiple vents or dikes in a given lava flow field. Magmas ascending through the crust as dikes are clearly oriented approximately parallel to other regional structures all forming in the same northeast-southwest oriented extensional stress regime (Kuntz *et al.*, 2002).

If the spatial distribution of basaltic volcanism on the ESRP is not strongly influenced by upper crustal structures then the geometry of melting in the source region may be the fundamental control. In fact, comparing the spatial density maps of vents on the ESRP (Figure 16.7) with mantle tomography shows a strong overlap between high vent intensity zones with thick (100–200 km) low velocity zones (e.g. Figure 2 of Yuan and Dueker, 2005). Zones of lesser intensity, such as along the southeastern margin of the Plain, also correspond with relatively high velocity, or colder regions of the upper mantle. Even the region of relatively low vent density SW of the TAN facility and the Lava Ridge–Hell's Half Acre VRZ overlaps in space with the a minor velocity increase in the upper mantle beneath that part of the ESRP. The Axial Volcanic Zone also overlies a region of low velocities in the upper mantle, as part of an ~ 250 km-long zone that extends SW from the Yellowstone Plateau (Saltzer and Humphreys, 1997). These observed correlations are similar to those made of the distribution of Quaternary volcanoes in Japan where they are confined to regions overlying hot mantle "fingers" (Tamura *et al.*, 2002; Tamura, Chapter 7, this volume; Kondo, Chapter 12, this volume) or low velocity zones. This relationship strongly suggests to us, as it does to Tamura and others, that the geometry of melting in the source plays the fundamental role in the distribution of volcanism at the surface.

Concluding remarks

The distribution of volcanoes on the surface on the ESRP has traditionally led to the interpretation that volcanism is focused into narrow, NW-trending zones

known as volcanic rift zones. However, based on recent stratigraphic data from the subsurface of the Plain within and immediately surrounding the INL, we can now test this view of ESRP volcanism, and more fully characterize the spatial variability in vent distributions, accumulation rates, and differential subsidence.

The results of this exercise demonstrate that volcanism is not focused into NW-trending volcanic rift zones, but rather is focused into a series of elongate, NE-trending zones along the NW margin and along the axis of the ESRP. The distribution of vents exposed at the surface of the Plain, by contrast, results from a complex interplay between variations in the intensity of volcanism and accumulation rates, plus local differential subsidence related to slip on Basin and Range normal faults that extend onto the ESRP. For example, in the area of the southern INL the distribution of vents at the surface suggests that volcanism is focused into the Arco–Big Southern Butte VRZ and the Axial Volcanic Zone and limited in the Big Lost Trough. In part, this distribution results from the differential subsidence and burial vents within the Big Lost Trough, while those in the Arco–Big Southern Butte VRZ are uplifted and have avoided burial. No variation in the density of volcanism or rate of basalt accumulation exists between these zones. The Axial Volcanic Zone south of the Big Lost Trough also subsided relative to the Arco–Big Southern Butte VRZ, but its topography has been maintained by a much higher rate accumulation rate relative to the other two zones.

Although the region surrounding the ESRP is seismically active, faults in the region are not spatially associated to any substantial degree with zones of high spatial density of volcanism on the Plain. There is, however, a strong spatial correlation between low velocity zones in the upper mantle and the zone of high spatial density of volcanism at the surface, suggesting that source geometry, and not near surface structures play, the fundamental role in determining the spatial distribution of vents.

This chapter was improved by the editorial comments of Chuck Connor and Neil Chapman.

References

Anderson, S. R. (1991). Stratigraphy of the unsaturated zone and uppermost part of the Snake River Plain aquifer at the Idaho Chemical Processing Plant and Test Reactors Area, Idaho National Engineering Laboratory, Idaho, USGS Water-Resources Investigations Report **91-4010**. US Geological Survey INL Project Office, ID.

Anderson, S. R. and R. C. Bartholomay (1995). Use of natural-gamma logs and cores for determining stratigraphic relations of basalt and sediment at the Radioactive Waste Management Complex, Idaho National Engineering Laboratory, Idaho. *Journal of the Idaho Academy of Science*, **31**, 1–10.

Anderson, S. R. and B. Bowers (1995). Stratigraphy of the unsaturated zone and uppermost part of the Snake River Plain aquifer at test area north, Idaho National Engineering Laboratory, Idaho, USGS Water-Resources Investigations Report **95-4130**. US Geological Survey INL Project Office, ID.

Anderson, S. R. and B. D. Lewis (1989). Stratigraphy of the unsaturated zone at the radioactive waste management complex, Idaho National Engineering Laboratory, Idaho, USGS Water-Resources Investigations Report **89-4065**. US Geological Survey INL Project Office, ID.

Anderson, S. R. and M. J. Liszewski (1997). Stratigraphy of the unsaturated zone and the Snake River Plain Aquifer at and near the Idaho National Engineering and Environmental Laboratory, Idaho, USGS Water-Resources Investigations Report **97-4183**. US Geological Survey INL Project Office, ID.

Anderson, S. R., M. J. Liszewski and L. D. Cecil (1997). Geologic ages and accumulation rates of basalt-flow groups and sedimentary interbeds in selected wells at the Idaho National Engineering Laboratory, Idaho, USGS Water-Resources Investigations Report **97-4010**(DOE/ID-22134). US Geological Survey INL Project Office, ID.

Anderson, S. R., D. J. Ackerman, D. J. Liszewski and R. M. Feiburber (1996). Stratigraphic data for wells at and near the Idaho National Engineering Laboratory, Idaho, USGS Open-File Report **96-248**. US Geological Survey INL Project Office, ID.

Bartholomay, R. C., L. C. Davis and P. K. Link (2002). Introduction to the hydrogeology of the eastern Snake River Plain. *In:* Link, P. K. and L. L. Mink (eds) *Geology, Hydrogeology, and Environmental Remediation; Idaho National Engineering and Environmental Laboratory, Eastern Snake River Plain, Idaho*, Special Paper **353**. Boulder, CO: Geological Society of America, 3–9.

Blair, J. J. (2002). Sedimentology and stratigraphy of sediments of the Big Lost Trough subsurface from coreholes at the Idaho National Engineering and Environmental Laboratory, Snake River Plain, Idaho. Unpublished M.S. thesis, Idaho State University.

Champion, D. E., M. A. Lanphere, S. R. Anderson and M. A. Kuntz (2002). Accumulation and subsidence of the Pleistocene basaltic lava flows of the eastern Snake River Plain, Idaho. *In:* Link, P. K. and L. L. Mink (eds) *Geology, Hydrogeology, and Environmental Remediation; Idaho National Engineering and Environmental Laboratory, Eastern Snake River Plain, Idaho*, Special Paper **353**. Boulder, CO: Geological Society of America, 175–192.

Connor, C. B., J. A. Stamatakos, D. A. Ferrill *et al.* (2000). Geologic factors controlling patterns of small-volume basaltic volcanism: Application to a volcanic hazard assessment at Yucca Mountain, Nevada. *Journal of Geophysical Research*, **105**(1), 417–432.

Connor, C. B., C. D. Condit, L. S. Crumpler and J. C. Aubele (1992). Evidence of regional structural controls on vent distribution: Springerville Volcanic Field, Arizona. *Journal of Geophysical Research*, **97**(B9), 12 349–12 359.

Conway, F. M., C. B. Connor, B. E. Hill, C. D. Condit, K. Mullaney and C. M. Hall

(1998). Recurrence rates of basaltic volcanism in SP clusters, San Francisco volcanic field, Arizona. *Geology*, **26**, 655–658.

Gianniny, G. L., G. D. Thackray, D. S. Kaufman *et al.* (2002). Late Quaternary highlands in the Mud Lake and Big Lost Trough sub-basins of Lake Terreton, Idaho. *In:* Link, P. K. and L. L. Mink (eds) *Geology, Hydrogeology, and Environmental Remediation: Idaho National Engineering and Environmental Laboratory, eastern Snake River Plain, Idaho*, Special Paper **353**. Boulder, CO: Geological Society of America, 77–90.

1 Gianniny, G. L., J. K. Geslin, J. W. Riesterer, P. K. Link and G. D. Thackray (1997). Quaternary surficial sediments near Test Area North northeastern Snake River Plain: An actualistic guide to aquifer characterization. *Proceedings of the 32nd Annual Symposium on Engineering Geology and Geotechnical Engineering*. Moscow, ID: University of Idaho, 29–44.

Hackett, W. R. and R. P. Smith (1994). Volcanic hazards of the Idaho National Engineering Laboratory and adjacent areas, Technical Report **INEL–94/0276**. Idaho Falls, ID: Idaho National Engineering Lab.

Hackett, W. R. and R. P. Smith (1992). Quaternary volcanism, tectonics and sedimentation in the INEL area. *In:* Wilson, J. R. (ed) *Field Guide to Geological Excursions in Utah and Adjacent Areas of Nevada, Idaho and Wyoming*. Salt Lake City, UT: Utah Geological Survey, 1–18.

Hayden, K. P. (1992). The geology and petrology of Cedar Butte, Bingham County, Idaho. Unpublished M.S. thesis, Idaho State University.

Hughes, S. S., M. McCurry and D. J. Geist (2002a). Geochemical correlations and implications for the magmatic evolution of basalt flow groups at the Idaho National Engineering and Environmental Laboratory. *In:* Link, P. K. and L. L. Mink (eds) *Geology, Hydrogeology and Environmental Remediation, Idaho National Engineering and Environmental Laboratory, Eastern Snake River Plain*, Special Paper **353**. Boulder, CO: Geological Society of America, 151–173.

Hughes S. S., P. H. Wetmore and J. L. Casper (2002b). Evolution of Quaternary tholeiitic basalt eruptive centers on the eastern Snake River Plain, Idaho. *In:* Bonnichsen, B., C. White and M. McCurry (eds) *Tectonic and Magmatic Evolution of the Snake River Plain Volcanic Province*, **B-30**. Moscow, ID: Idaho Geological Survey, 363–385.

Kuntz, M. A. (1992). A model-based perspective of basaltic volcanism, eastern Snake River Plain, Idaho. *In:* Link, P. K., M. A. Kuntz and L. B. Platt (eds) *Regional Geology of Eastern Idaho and Western Wyoming*. Boulder, CO: Geological Society of America, 289–304.

Kuntz, M. A. (1977a). Extensional faulting and volcanism along the Arco rift zone, eastern Snake River Plain, Idaho. *Geological Society of America Abstracts with Programs*, **9**, 740–741.

Kuntz, M. A. (1977b). Rift zones of the Snake River Plain, Idaho, as extensions of basin-range and older structures. *Geological Society of America Abstracts with Programs*, **9**, 1061–1062.

Kuntz, M. A., S. R. Anderson, D. E. Champion, M. A. Lanphere and D. J. Grunwald (2002). Tension cracks, eruptive fissures, dikes, and faults related to late Pleistocene-Holocene basaltic volcanism and implications for the distribution of hydraulic conductivity in the eastern Snake River Plain. *In:* Link, P. K. and L. L. Mink (eds) *Geology, Hydrogeology, and Environmental Remediation: Idaho National Engineering and Environmental Laboratory, eastern Snake River Plain, Idaho*. Boulder, CO: Geological Society of America, Special Paper **353**, 111–133.

Kuntz, M. A., B. Skipp, M. A. Lanphere, *et al.* (1994). Geologic map of the Idaho Na-

tional Engineering Laboratory and adjoining areas, eastern Idaho, **I-2330**. Moscow, ID: Idaho Geological Survey.

Kuntz, M. A., H. R. Covington and L. J. Schorr (1992). An overview of basaltic volcanism of the eastern Snake River Plain, Idaho. *In:* Link, P. K. , M. A. Kuntz and L. B. Platt (eds) *Regional Geology of Eastern Idaho and Western Wyoming*. Boulder, CO: Geological Society of America, 227–267.

Kuntz, M. A., D. E. Champion, E. C. Spiker and R. H. Lefebvre (1986). Contrasting magma types and steady-state, volume-predictable basaltic volcanism along the Great Rift, Idaho. *Geological Society of America Bulletin*, **97**(5), 579–594.

McCurry, M., K. P. Hayden, L. H. Morse, S. Mertzman (2008). Genesis of post-hotspot, A-type rhyolite of the Eastern Snake River Plain volcanic field by extreme fractional crystallization of olivine tholeiite. *Bulletin of Volcanology*, **70**, 361–383.

McCurry, M. O., W. R. Hackett and K. P. Hayden (1999). Cedar Butte and cogenetic Quaternary rhyolite domes of the eastern Snake River Plain. *In:* Hughes, S. S. and G. D. Thackray (eds) *Guidebook to the Geology of Eastern Idaho*. Pocatello, ID: Idaho Museum of Natural History and Idaho State University Press, 169–179.

McQuarrie, N. and D. W. Rodgers (1998). Subsidence of a volcanic basin by flexure and lower crustal flow: eastern Snake River Plain, Idaho. *Tectonics*, **17**, 203–220.

Pierce, K. L. and L. A. Morgan (1992). The track of the Yellowstone Hotspot: volcanism, faulting, and uplift. *In:* Link, P. K. , M. A. Kuntz and L. B. Platt (eds) *Regional Geology of Eastern Idaho and Western Wyoming*, Memoir **179**. Boulder, CO: Geological Society of America, 1–53.

Saltzer, R. L. and E. D. Humphreys (1997). Upper mantle P wave velocity structure of the eastern Snake River Plain and its relationship to geodynamic models of the region. *Journal of Geophysical Research*, **102**(B6), 11 829–11 841.

Scarberry, K. C. (2003). Volcanology, geochemistry and stratigraphy of the F basalt flow group, eastern Snake River Plain, Idaho. Unpublished M.S. thesis, Idaho State University.

Tamura, Y., Y. Tatsumi, D. Zhao, Y. Kido and H. Shukuno (2002). Hot fingers in the mantle wedge: new insights into magma genesis in subduction zones. *Earth and Planetary Science Letters*, **197**, 105–116.

Wetmore, P. H. (1998). An assessment of physical volcanology and tectonics of the central eastern Snake River Plain based on the correlation of subsurface basalts at and near the Idaho National Engineering and Environmental Laboratory, Idaho. Unpublished M.S. thesis, Idaho State University.

Wetmore, P. H., S. S. Hughes, D. W. Rodgers and S. R. Anderson (1999). Constructional origin of the Axial Volcanic Zone of the eastern Snake River Plain, Idaho. *Geological Society of America Abstracts with Programs*, *31*(4), 61.

Wetmore, P. H., S. S. Hughes and S. R. Anderson (1997). Model morphologies of subsurface Quaternary basalts as evidence for a decrease in the magnitude of basaltic magmatism at and near the Idaho National Engineering and Environmental Laboratory, Idaho. *Proceedings of the 32nd Symposium on Engineering Geology and Geotechnical Engineering*, 45–58.

Yuan, H. and K. Dueker (2005). Teleseismic P-wave tomogram of the Yellowstone plume. *Geophysical Research Letters*, **32**, L07304, doi:10.1029/2004GL022056.